applied sciences

MDPI

Article

Research on Pure Hydrogen Production Using a Fuel-Processing System Combined with a PSA System

Seokkyun Ko and Sangyong Lee *

Mechanical Robotics and Energy Department, Dongguk University, Seoul 04620, Republic of Korea
* Correspondence: sangyonglee@dongguk.edu

Abstract: Research was conducted to improve the system efficiency of a fuel-processing system combined with a hydrogen-purification system to supply hydrogen to a 10 kW residential building proton-exchange membrane fuel cell (PEMFC). The system consists of a steam-reforming reactor, a water–gas shift reactor, heat exchangers and a pressure swing adsorption (PSA) system, increasing the purity of the produced hydrogen by over 99.97%. Aspen Plus® and Aspen adsorption® simulators were used to optimize operating conditions by calculating thermal efficiency and hydrogen-production yield under various temperature and pressure conditions in the reformer. To optimize the hydrogen-production system, simulations were performed under conditions of 1 to 10 atm and 600 to 1000 °C, and simulations were also performed while maintaining the PSA pressure at 9 atm. The overall system efficiency was expressed as a function of methane conversion, and the methane conversion was expressed as a function of reformer temperature and pressure. The fuel-processing system showed the highest thermal efficiency of 82.40% at a pressure of 1 atm and a temperature range of 800 °C. For the combined system of a fuel-processing system and a hydrogen-purification system, the highest hydrogen-production yield was 43.17% at 800 °C and 1 atm.

Keywords: hydrogen production; hydrogen processing system; PSA

check for updates

Citation: Ko, S.; Lee, S. Research on Pure Hydrogen Production Using a Fuel-Processing System Combined with a PSA System. *Appl. Sci.* **2023**, *13*, 11947. https://doi.org/10.3390/app132111947

Academic Editor: Jose Miguel Campos-Martin

Received: 4 October 2023
Revised: 26 October 2023
Accepted: 28 October 2023
Published: 1 November 2023

Copyright: © 2023 by the authors. Licensee MDPI, Basel, Switzerland. This article is an open access article distributed under the terms and conditions of the Creative Commons Attribution (CC BY) license (https://creativecommons.org/licenses/by/4.0/).

1. Introduction

Energy consumption in public buildings and general households is gradually increasing [1]. Lombard and his colleagues predict that energy consumption will increase from 6500 Mtoe in 2020 to about 7500 Mtoe in 2025 [1]. As energy consumption increases, so do carbon emissions, and there is an increasing need to develop new methods to reduce CO_2 emissions. Distributed power generation is one of the possible solutions [2–6], which is a form of power generation that directly generates and supplies power in areas where power supply is needed [7,8]. Distributed power generation includes photovoltaic power generation, wind power generation, cogeneration using waste heat recovery, and fuel cells [9,10]. Fuel cells for residential buildings and homes are a representative form of distributed power generation since they have a relatively small installation area compared to other renewable energy systems and can utilize existing urban natural gas infrastructure when combined with a fuel-processing system [7,8,10,11]. Accordingly, hydrogen fuel cells are attracting attention as an emergency power source for power since they produce a large amount of power per unit area and are easy to install [12]. Therefore, the demand for fuel cell systems for residential buildings is increasing worldwide, and their electricity output, durability, system size, and cost for system installation and operation are becoming competitive [1,13]. Additionally, the fuel cell produces electrical energy and thermal energy through electro-chemical reactions of hydrogen and does not emit harmful substances; it only emits water. Also, fuel cells are high-efficiency power generation systems with an overall efficiency of around 50% and over 70% if combined with a heat recovery system, while conventional primary energy systems such as coal and oil have a conversion efficiency of about 31% [14]. Fuel cells have the advantage of continuously producing energy without

affecting the environment compared to other renewable energy sources. Commonly used types of fuel cells include PEMFCs (Polymer Electrolyte Membrane Fuel Cells), DMFCs (Direct Methanol Fuel Cells), SOFCs (Solid Oxide Fuel Cells), and MCFCs (Molten Carbonate Fuel Cells). Among them, PEMFCs operate at a relatively lower temperature than other types of fuel cells, have a high-power density, have a simple structure with excellent space efficiency, and have power production flexibility [15]. Hydrogen fuel cells are expected to be a next-generation energy source and are expected to be in high demand [16,17]. Because of these advantages, they are the most commercialized and are mainly used as fuel cells for homes and residential buildings [18].

The growing demand for hydrogen for residential buildings has had a significant impact on the development of hydrogen-production processes for fuel cell systems in residential buildings [1]. Widely used hydrogen-production methods include water electrolysis methods, which electrolyze water to produce hydrogen; the ammonia photolysis method, which irradiates light through a bulb to decompose ammonia into hydrogen and nitrogen; and the hydrocarbon reforming method, which extracts hydrogen from various hydrocarbons such as methanol, ethanol, LNG (Liquefied Natural Gas) and PNG (Pressurized Natural gas). Reforming processes are the most popular hydrogen-production methods and include autothermal reforming, partial oxidation reforming, steam reforming, and ethanol reforming [17,19–21].

Among them, the natural gas steam-reforming system has the advantage of relatively high hydrogen production, the lowest unit hydrogen-production cost and stable operation, making it the most commonly used technology for industrial use [17,22,23]. As the residual fuel cell system increases, it is needed to maximize the efficiency of the hydrogen-production system [17,21].

The natural gas steam-reforming system consists of a steam-reforming reactor, a water gas shift (WGS) reactor and a preferential oxidation reactor (PROX). In the steam-reforming process, natural gas and steam react to form hydrogen, along with carbon monoxide and carbon dioxide. Reformate gas is further reacted with water in the water–gas shift reactor and produces additional hydrogen and carbon dioxide from CO and water. After the water–gas shift reaction, the concentration of hydrogen of the product gas would be around 75% and the concentration of CO_2 is around 20%, with a very small amount of CO and unreacted hydrocarbons [12,23,24]. If carbon monoxide is introduced to the polymer-exchange membrane fuel cell (PEMFC) along with hydrogen, carbon monoxide reacts with the platinum catalyst of the fuel cell and acts as a poison, reducing the performance and durability of the fuel cell, and the carbon dioxide also acts as a poison in the anode [25,26]. The allowable concentration of carbon monoxide is 10 ppm in a normal state and 100 ppm in an excessive state. Also, CO_2 is emitted from the steam-reforming process, which needs to be separated and stored or utilized. Therefore, high-purity hydrogen is required as a fuel in PEMFCs, and hydrogen-purification systems must be combined [17,21,27–29], which requires the development of a separation and purification process [30]. Existing technologies include a low-temperature distillation method, a non-porous polymer membrane method, a preferential oxidation (PROX) reaction method and an adsorption method (PSA: Pressure Swing Adsorption, TSA: Temperature Swing Adsorption).

The hydrogen separation and purification process using the swing adsorption method is an energy-saving process without a phase transition for the mixture and enables separation and recovery at the same time [31,32]. In addition, it is a process that enables precise separation at the molecular level through the pore size and surface treatment of the adsorbent, and it has technical advantages when applied to small- to large-scale processes. With the swing adsorption method, CO_2 that cannot be removed from the PROX reactor also can be removed and used as a carbon capture and storage (CCS) method. In addition to these advantages, a PSA system was selected as a hydrogen-purification method, possessing additional advantages of relatively low operating costs, easy operation, and easy automation of the process in the commercialization process [31–33].

In this study, the PSA system was applied for hydrogen purification to obtain over 99.97% pure hydrogen. The PSA system purifies hydrogen by adsorbing and desorbing substances other than hydrogen, depending on the diffusivity, molecular weight, and density of the gas, by repeating the adsorption and desorption of two or more chambers crossing each other [31,33]. For hydrogen production, a fuel-processing system was applied.

Much research has been conducted on fuel-processing systems and PSA systems, respectively. However, there is not much research on systems combining fuel-processing and PSA systems and economical pure-hydrogen-production methods, especially at the small and medium scale [31,32]. In this study, we combined two cost-effective systems—the methane steam reforming system and the PSA system—for small- to medium-sized pure hydrogen production and investigated the influence of various thermodynamic parameters on the overall system efficiency using Aspen Plus® and Aspen Adsorption®. The concentration of gas discharged from the fuel-processing system varies depending on the temperature and pressure conditions of the reformer, which affect the hydrogen-purification efficiency of PSA systems. During PSA operation, the pressure of the PSA system was maintained at 9 atm, and the use of a compressor was essential depending on the operating pressure of the fuel-processing system.

The combined system was analyzed using the following:

(1) Efficiency analysis according to the temperature and pressure of the fuel-processing system.
(2) Purification efficiency analysis according to PSA injection gas composition.
(3) Selection of optimal operating conditions through efficiency analysis according to the operating conditions of the fuel-processing and PSA combined system.

For optimizing the process of producing hydrogen with a purity of 99.97% or higher by linking the PSA system to the existing fuel-processing process, the overall thermal efficiency and the hydrogen-production yield were analyzed.

2. Theoretical Background

The system for producing high-purity H_2 consists of a methane reformer, a water–gas shifter, and a pressure swing adsorber. Theoretical calculations for the system were performed using the following assumptions.

I. The steam-reforming reaction and the water–gas shift reaction in the reformer are considered to have reached chemical equilibrium at the reactor outlet.
II. The water–gas shift reaction in the water–gas shift reactor reaches chemical equilibrium at the outlet of the reactor.

3. Methane Steam-Reforming Reaction/WGS Reaction

The steam-reforming reaction is an endothermic reaction in which natural gas reacts with steam to produce hydrogen and carbon monoxide, while the water–gas shift reaction is an exothermic reaction in which carbon monoxide reacts with steam to produce additional hydrogen and carbon dioxide. There are more than 11 chemical reactions in the reformer internal reaction, including the steam-reforming reaction, the water–gas shift reaction, the carbon dioxide reforming reaction, the methanation reaction, and the methane decomposition reaction, which are summarized in Table 1 [34,35].

Among those reactions, two main reactions were considered to calculate the concentration of each gas at the exit stream of the steam reformer, assuming that these two reactions are dominant reactions [36,37]. In the water–gas shift reactor, only the water–gas shift reaction is considered [36,37]. In the water–gas shift reactor, CO concentration is reduced to less than 0.05% [23,37,38].

Table 1. Possible reactions in methane steam reforming.

	Reactions	Energy Amount
Steam reforming	$CH_4 + H_2O \rightarrow CO + 3H_2$	$\Delta H^0_{298K}\text{Jmol}^{-1} = 205,800$
Steam reforming + Water–gas shift	$CH_4 + 2H_2O \rightarrow CO_2 + 4H_2$	$\Delta H^0_{298K}\text{Jmol}^{-1} = 164,600$
Dry reforming	$CH_4 + CO_2 \rightarrow 2CO + 2H_2$	$\Delta H^0_{298K}\text{Jmol}^{-1} = 247,000$
Combustion	$CH_4 + 2O_2 \rightarrow CO_2 + 2H_2O$	$\Delta H^0_{298K}\text{Jmol}^{-1} = -802,600$
Partial oxidation	$CH_4 + 0.5O_2 \rightarrow CO + 2H_2$	$\Delta H^0_{298K}\text{Jmol}^{-1} = -36,000$
CO oxidation	$CO + 0.5O_2 \rightarrow CO_2$	$\Delta H^0_{298K}\text{Jmol}^{-1} = -282,993$
Hydrogen oxidation	$H_2 + 0.5O_2 \rightarrow H_2O$	$\Delta H^0_{298K}\text{Jmol}^{-1} = -241,856$
Water–gas Shift	$CO + H_2O \rightarrow CO_2 + H_2$	$\Delta H^0_{298K}\text{Jmol}^{-1} = -41,200$
Methanation I	$CO + 3H_2 \rightarrow CH_4 + H_2O$	$\Delta H^0_{298K}\text{Jmol}^{-1} = -205,800$
Methanation II	$CO_2 + 4H_2 \rightarrow CH_4 + 2H_2O$	$\Delta H^0_{298K}\text{Jmol}^{-1} = -164,600$
Methanation III	$CO_2 + H_2 \rightarrow CH_4 + CO_2$	$\Delta H^0_{298K}\text{Jmol}^{-1} = -247,000$
Endothermic water–gas shift	$CO_2 + H_2 \rightarrow CO + H_2O$	$\Delta H^0_{298K}\text{Jmol}^{-1} = 41,200$
Methane decomposition	$CH_4 \rightarrow C + 2H_2$	$\Delta H^0_{298K}\text{Jmol}^{-1} = 74,500$

To calculate the outlet composition for each reactor, equilibrium constants in Equations (1) and (2) are applied, respectively.

$$K_{SR} = \frac{p_{CO}\ {p_{H_2}}^3}{p_{CH_4} p_{\ H_2}\ atm^2} \quad (1)$$

$$K_{WGS} = \frac{p_{H_2}\ p_{CO_2}}{p_{H_2O}\ p_{CO}} \quad (2)$$

Equation (1) represents the formula for the steam-reforming reaction, and Equation (2) represents the formula for the water–gas shift reaction. In Equations (1) and (2), K_{SR} represents the equilibrium constant for the steam-reforming reaction, and K_{WGS} represents the equilibrium constant for the water–gas shift reaction, which are temperature-dependent variables. These equilibrium constants have been compiled and are listed in Table 2 [39]. Also, p_x denotes the partial pressure of component x. Based on this information, it is possible to determine the composition at an equilibrium state using equilibrium constants and partial pressure. For reforming reactors, Ni-based catalysts are used to prevent carbon decomposition in the temperature range of 500 °C to 800 °C. However, above 600 °C and up to 1100 °C, Ru-based catalysts are used [23,40,41]. For water–gas shift reactors, Cr-based and Cu-based catalysts are predominantly used and are operated within the temperature range of 150 °C to 350 °C [41].

Table 2. Equilibrium constant for temperature.

Temperature (°C)	K_{SR}	K_{WGS}
400	5.93×10^{-8}	1.17
600	5.22×10^{-1}	2.55
800	1.69×10^{2}	1.04
1000	1.0934×10^{-4}	0.58

4. PSA (Pressure Swing Adsorption) System

When a gas is physically adsorbed into a solid surface, an adsorption equilibrium is achieved between gas molecules and the adsorbed sites on the surface of the adsorbent (activated carbon). The expression of the coverage is defined as the ratio of the area occupied by gas molecules to the total surface area of the adsorbent, which depends on the partial pressure of the gas and is called the adsorption isotherm [42,43].

To calculate the adsorption isotherm, several models have been proposed, such as the Langmuir isotherm, the Langmuir–Freundlich isotherm, IASR, DSL, and VSM. Among

them, the Langmuir and Langmuir–Freundlich isotherms are commonly used to predict the adsorption equilibrium compared to the IAST (Ideal Adsorbed Solution Theory) or VSM (Vacancy Solution Model) models, which have a large number of parameters and relatively complex equations [42,43]. DSL (Dual-Site Langmuir) also has many parameters, but its shape is similar to the existing Langmuir model, which is not complicated and is easy to predict [42,43]. Understanding the dynamics of adsorption beds filled with porous particles such as zeolites or activated carbon in PSA processes is essential for understanding mathematical models for controlling and estimating hydrogen purification [27].

For the analysis of the PSA system, the mass balance and energy balance were calculated along with the extended Langmuir isotherm for gas consumption using the following assumptions [31,32].

(1) Radial gradients for flow velocity, concentration, and temperature can be ignored, and the flow of fluid is a one-dimensional plug flow.
(2) There is no pressure drop due to friction between the fluid and the adsorbent in the chamber.
(3) The temperature of the adsorbent is constant at any point, and there is always a thermal equilibrium between the fluid and the adsorbent.
(4) The main resistance of material transfer exists in the adsorbent, and the external epidural material transfer resistance is ignored.

Based on the assumptions, the following mass balance and energy balance equations were set and used in the simulation [31,32].

$$\frac{RT}{P}\rho\left(\frac{1-\varepsilon}{\varepsilon}\right)\frac{\partial q_i}{\partial t}+\frac{\partial(uy_i)}{\partial z}-D_{ax}\frac{\partial^2 y_i}{\partial z^2}=0 \tag{3}$$

$$\begin{aligned}\left(\varepsilon_b cC_{pg}+(1-\varepsilon_b)\rho_p C_{ps}\right)\frac{\partial T}{\partial t}= \; & -\varepsilon_b cC_{pg}U_z\frac{\partial T}{\partial z}+K_Z\frac{\partial^2 T}{\partial z^2}+(1-\varepsilon_b)\rho_p\sum_{j=1}^{N}\left(\Delta H_j\frac{\partial q_j}{\partial t}\right)\\ & -\varepsilon\frac{2h_{in}}{R_{in}}(T-T_w)\end{aligned} \tag{4}$$

The mass balance equation can be written as Equation (3) and the energy balance equation is written as Equation (4). In the mass balance equation, the RT/P is the equation of state, ε represents the volume fraction in the mixture, $\frac{\partial q_i}{\partial t}$ represents the rate of change over the time of component i, $\frac{\partial(uy_i)}{\partial z}$ represents the mass flow in the vertical direction, and D_{ax} represents the diffusion rate of component i. In the energy balance equation, ε is the volume fraction, C_p is the heat capacity, U_z is the speed of the fluid, $\frac{\partial T}{\partial z}$ is the rate of temperature change in the z direction, K_Z is the effective axial thermal conductivity, and H_j is the reaction enthalpy.

To calculate the number of gas molecules adsorbed per unit of adsorbent in the chamber, the extended Langmuir isotherm is applied, and it is given as the following equation.

$$q=\frac{q_{mi}B_iP_i}{1+\sum_j^N B_jP_j} \tag{5}$$

where q represents the number of moles of gas molecules adsorbed per unit mass of adsorbent and q_m represents the maximum adsorption amount of gas as a parameter. B_i is the Langmuir isotherm parameter of species i and P_i is the partial pressure of species i. The amount of saturated adsorption is given as the following equation.

$$q_m=a_1+a_2T \tag{6}$$

$$B=b_0\exp\left(\frac{b_1}{T}\right) \tag{7}$$

Parameters according to the adsorbent applied to the PSA system are shown in Table 3 [44].

Table 3. Langmuir parameters for activated carbon and zeolite.

Langmuir Parameters						
Component	a_{i1} **(mol/kg)**	$a_{i2}\times10^2$ **(mol/K/kg)**	$b_{i1}\times10^4$ **(1/bar)**	b_{i1} **(K)**	k_i**(1/s)**	ΔH_i**(cal/mol)**
activated carbon						
H_2	163,943	−2.1	0.6248	1229	0.7	2880
CO	33.85	−9.072	2.311	1751	0.15	4300
CH_4	23.86	−5.621	34.78	1159	0.195	4290
CO_2	28.7973	−7	100	1030	0.0355	5240
Zeolite 5A						
H_2	4.314	−1.06	25.15	458	0.7	2800
CO	11.8454	−3.13	202	763	0.063	5000
CH_4	5.833	−1.192	6.0504	1731	0.147	5300
CO_2	10.03	−1.858	15,781	207	0.0135	9330

5. Simulation Results

The entire simulation process is in Figure 1. The simulation was conducted in two parts: The fuel-processing system and the hydrogen-purification system.

(1) The fuel-processing system consists of a reformer, a water–gas shift reactor and three heat exchangers and is simulated with an Aspen Plus® simulator using a chemical equilibrium model.

(2) The hydrogen-purification system employs a PSA system, which is simulated by an Aspen Adsorption® simulator, where kinetic models are employed.

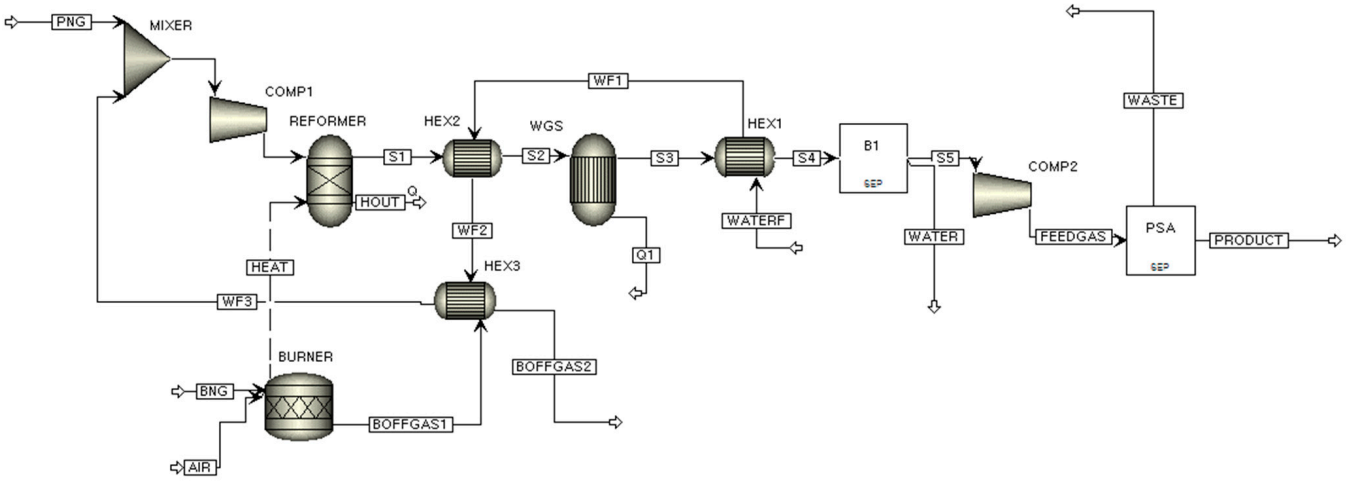

Figure 1. Overall process flowsheet.

6. Reformer, WGS Reactor Simulation

The simulations were performed using the Aspen Plus® simulator for the reformer and WGS reactor. In the simulation, the Peng–Robinson equation of state is employed to calculate the thermodynamic properties of the gas, and the steam-table method is employed to calculate the water properties, which is available in the Aspen Simulator [36]. In a reformer, the methane reforming reaction and the water–gas shift reaction are considered, and both reactions are considered to be in reaction equilibrium at given temperature and pressure conditions, assuming that the reactor is large enough to have sufficient residence time. As a raw material for hydrogen production, pure methane was introduced into the

fuel processor at 15 °C and 1 atm during simulations. The simulations were performed at temperatures from 600 °C to 1000 °C and a pressure of 1 atm to 10 atm. Simulations for the WGS reactor were conducted at 200 °C and at a pressure corresponding to that of the reformer. The gas flow rate of methane was controlled between 30 lpm and 61 lpm tor, making 10 kW of H2. The simulation conditions for the pure processing system are summarized in Table 4. The amount of methane supplied to the process is the summation of process natural gas (PNG) and burner natural gas (BNG). At this time, PNG refers to natural gas used in reforming reactors and BNG refers to natural gas used in burners for heat duty. The PNG flow rate is controlled to make 10 kW at given temperature and pressure conditions.

Table 4. Operating conditions for Aspen Plus® simulation.

Simulation Conditions	
Reformer temperature (°C)	600–1000
Reformer pressure (atm)	1–10
Water–gas shift temperature (°C)	200
Input gas temperature (°C)	15
Total input methane gas amount (lpm)	30–61
Compressor efficiency	0.8
Steam-carbon ratio (S/C ratio)	3

In the case of the water–gas shift reactor, only the water–gas shift reaction was considered when calculating the equilibrium composition under the given temperature and pressure conditions. For heat recovery, three shortcut heat exchangers were added, as shown in Figure 1. Heat exchanger B5 is a heat exchanger for cooling the reformed gas temperature to the operating temperature of the WGS reactor, and B2 is a heat exchanger for making the outlet reformed gas temperature the same as the PSA inlet temperature. Any remaining water at the outlet of the water–gas shift reactor must be removed for the PSA process. Heat exchanger B2 and water separator B1 are added to the simulation for water removal by condensation. In the PSA process, over 99.97% hydrogen is produced, where the operating conditions for the hydrogen-purification system are 15 °C and 9 atm.

Figure 2 shows the simulation results of each gas composition in the WGS reactor outlet flow according to the reformer temperature. As is shown in the figure, the concentration of H2 increases as the reformer temperature increases. Since the operating pressure of PSA is 9 atm for hydrogen purification, a compressor is needed to increase the pressure of the stream entering the PSA to 9 atm. The efficiency of the compressor was calculated as a mechanical efficiency of 0.8 and an isentropic efficiency of 0.8 [45].

The reaction equilibrium assumption was applied to the reforming reaction and the WGS reaction. Reformer temperatures of 600 °C to 1000 °C and pressures of 1 atm to 10 atm were simulated to investigate the effects of temperature and pressure on product gas composition. The WGS temperature was fixed at 200 °C at the pressure of 1 atm to 10 atm, and the steam-to-carbon ratio at the inlet stream to the reformer was fixed at 3. Concentration changes for each gas due to temperature change at 1 atm in the WGS reactor outlet are listed in Figure 2. Since the methane reforming reaction occurs in a reformer only, the amount of unreacted methane decreases as the reformer temperature increases.

Figure 3 shows the change in concentration of H2 and CO according to the change in the temperature of the reformer (from 600 °C to 1000 °C) and the change in process pressure (from 1 atm to 10 atm). As is shown in the figure, the concentration of hydrogen increased as the temperature of the reformer increased, but it appeared to stabilize at a temperature of 750 °C to 950 °C depending on the process pressure. This is because the equilibrium constant is an exponential function of the reciprocal of temperature and has a smaller value at high pressures due to Le Chatelier's law.

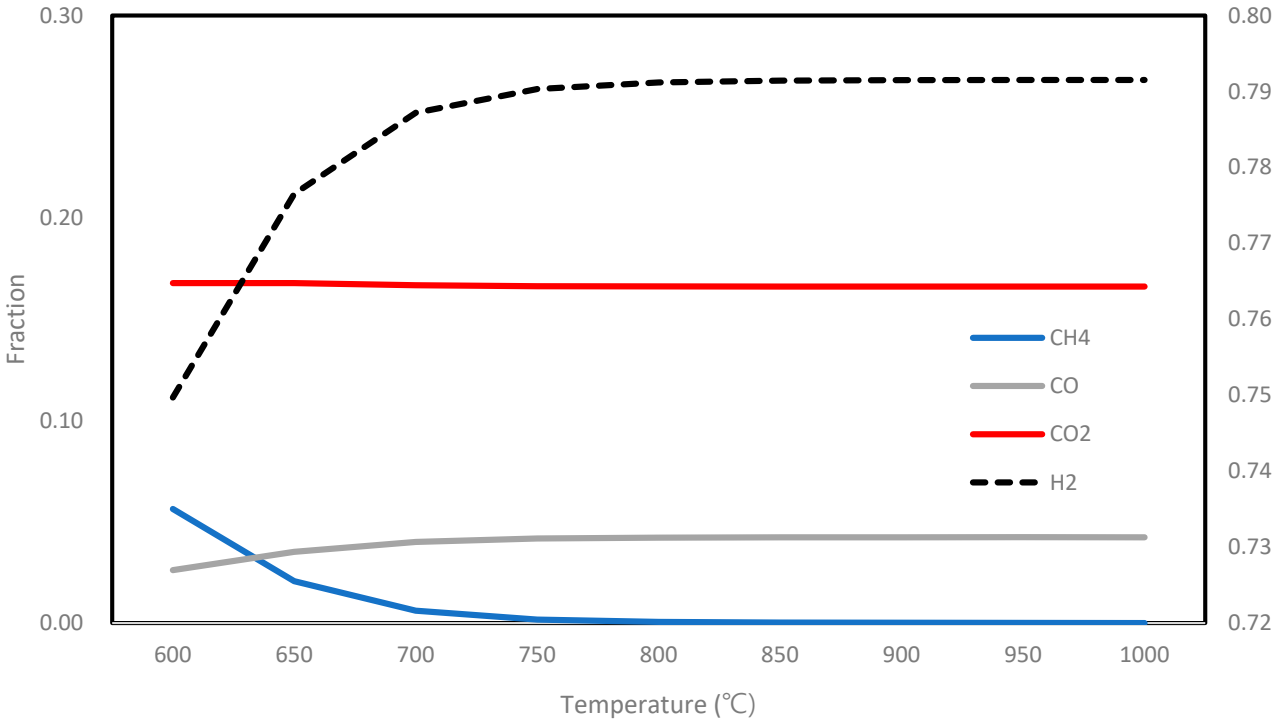

Figure 2. Gas composition change at WGS outlet according to reformer T.

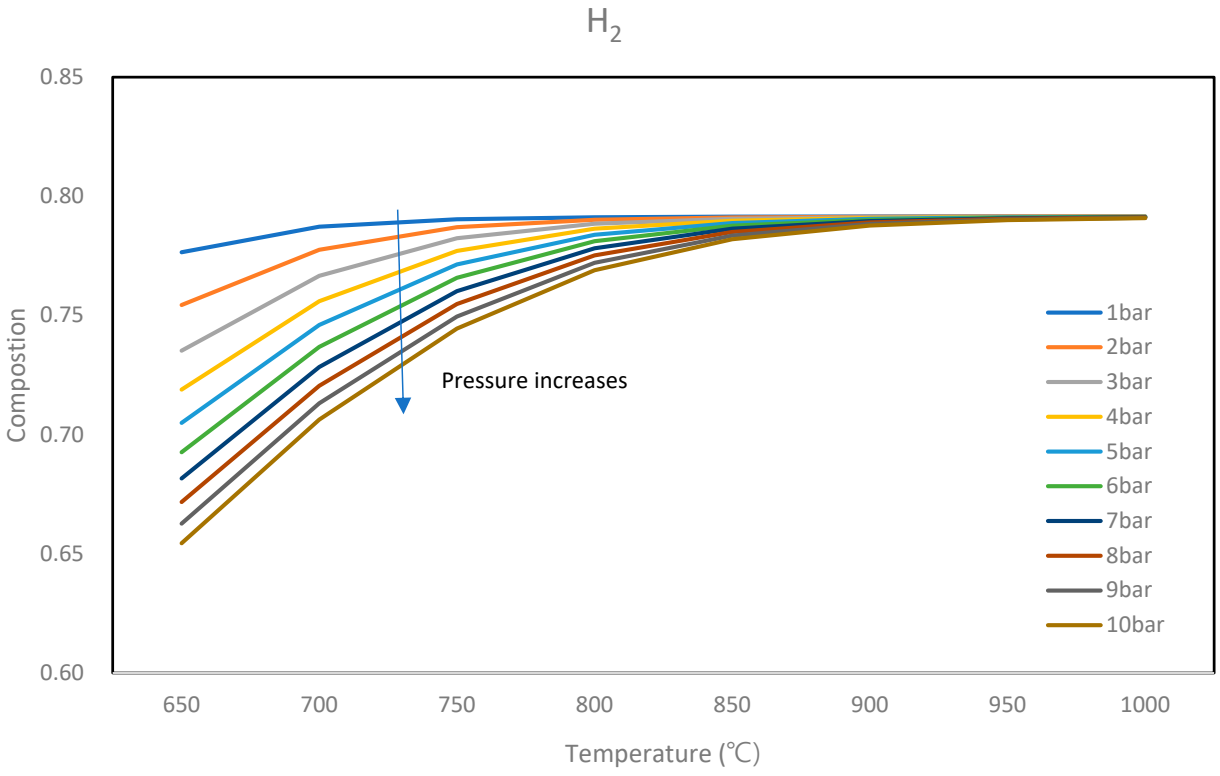

Figure 3. *Cont.*

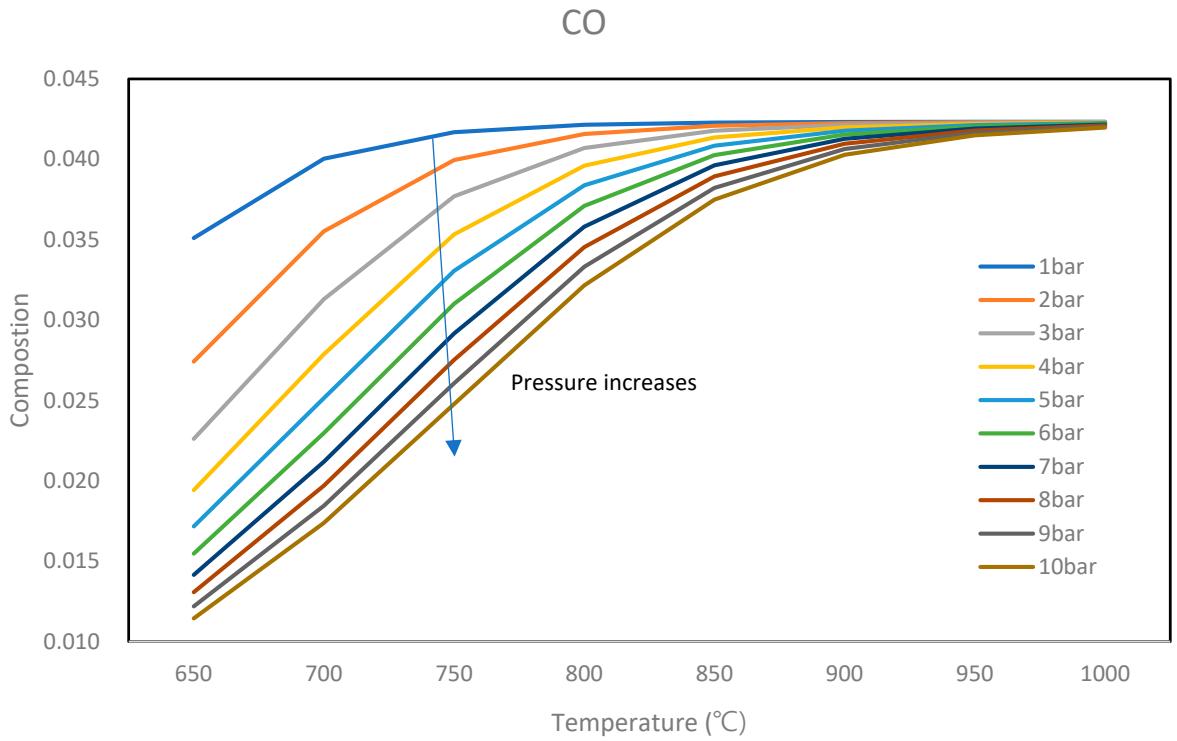

Figure 3. Variations of composition by gas according to temperature and pressure.

Simulations of CH4 conversion at various reformer temperatures and system pressures are shown in Figure 4. The conversion ratio of CH_4 increases with increasing temperature and decreases with increasing pressure. Since the conversion rate of CH_4 is an endothermic reaction, it increases as the temperature increases, and according to Le Chatelier's law, the conversion ratio decreases as the pressure increases.

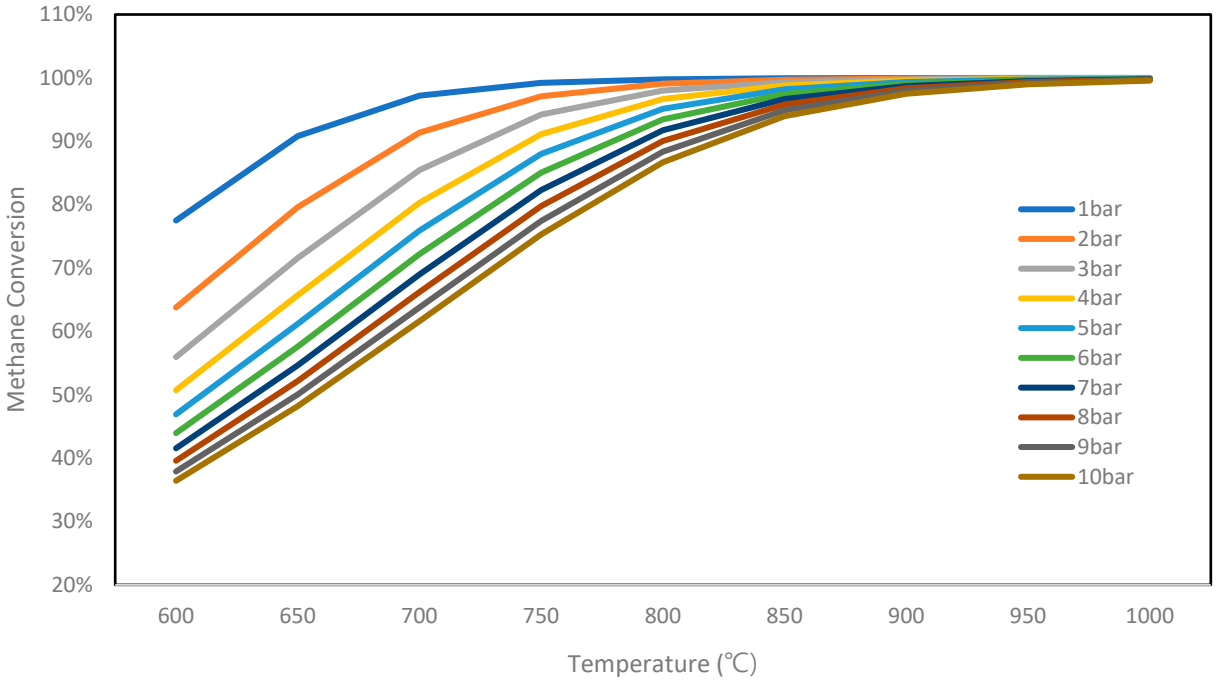

Figure 4. Methane conversion according to temperature and pressure.

As the conversion of CH_4 increases, the products of the steam-reforming reaction increase and the concentrations of H_2 and CO increase, as shown in Figure 3 [39].

7. Reformer Heat Duty

The heat of the reaction for the steam-reforming reaction under various temperature and pressure conditions and the heating energy required to bring the reactant temperature to the reformer temperature without a heat exchanger were calculated; they are summarized in Figure 5. For all simulations, PNG flow rates and BNG flow rates were used to produce 10 kW hydrogen through the methane reforming reaction and the WGS reaction. Because more methane is needed to make 10 kW of hydrogen at lower conversions, and less methane is needed at higher conversions, the heat duty required at low methane conversions is higher than at higher conversions. With these heat duties, the amount of heat to supply to the burner as well as the flow rate of methane introduced to the burner as a fuel would be calculated at a given methane conversion. If the heat exchanger is added to the process, the heat loss generated by the burner and the process can be minimized, which can reduce heat duty and increase efficiency. Therefore, three heat exchangers were added to the entire process, which were placed at each outlet of the reformer, the WGS reactor, and the burner.

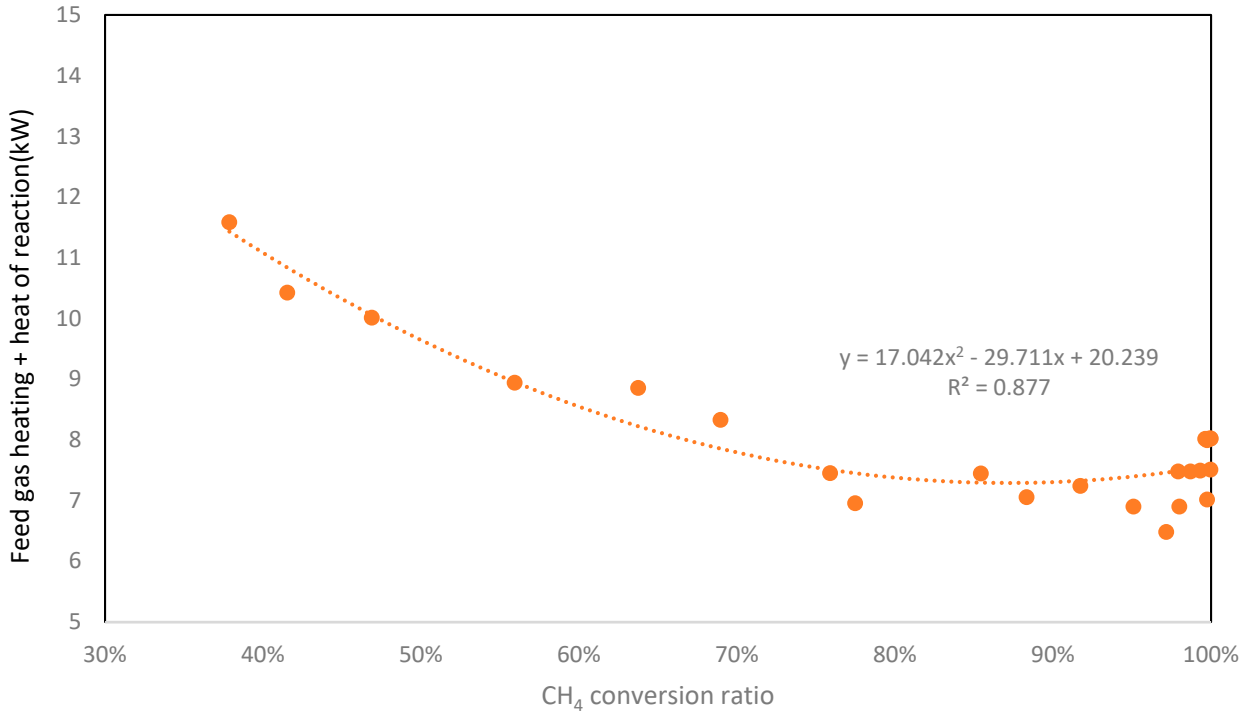

Figure 5. Reformer heat duty at the methane-conversion ratio in the reformer.

Total flow rate is the sum of the flow rate of BNG and the flow rate of PNG, which is shown in Figure 6. As is mentioned, a higher flow rate of PNG is needed at a lower methane conversion to make 10 kW hydrogen, since a small portion of PNG is converted into H_2. At the low conversion of PNG, most of the heat supplied by BNG is used to heat the reactants for the steam-reforming reaction, while a small amount of heat is used to heat the steam-reforming reaction. At the high conversion of CH_4, most of the heat supplied by BNG is used for the heat of reaction of steam methane reforming, since less PNG is needed.

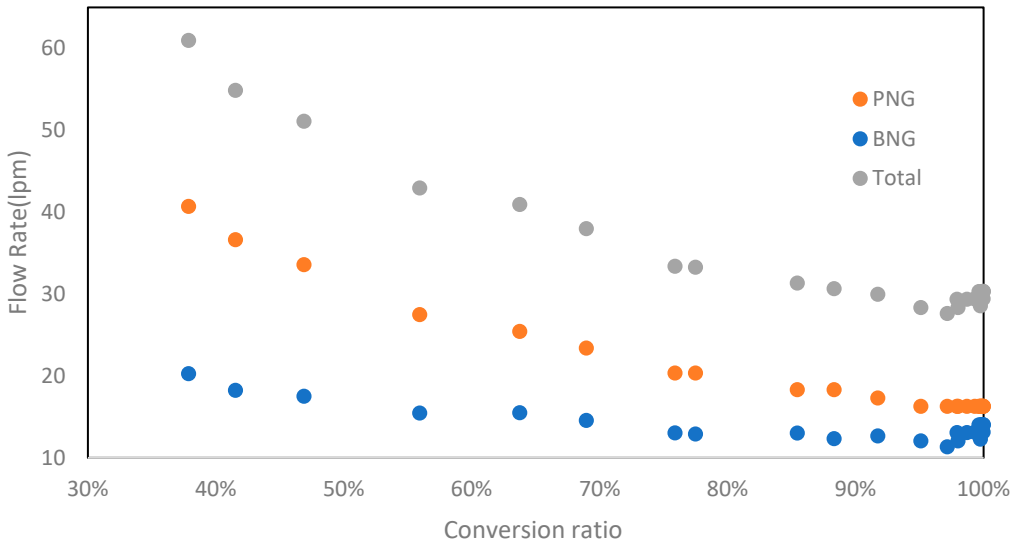

Figure 6. Methane gas flow rate.

8. Calculation of Reformer Efficiency According to S/C Ratio

The methane conversion at the reformer varies depends on the steam-to-carbon (S/C) ratio—that is, the ratio between numbers of moles of water and the number of moles of carbon in the PNG. The efficiency was calculated with simulation results to determine the optimal S/C ratio. Figure 7 shows the results of calculating the S/C ratios as 2, 3, and 4, respectively. The maximum yield of 79.51% was obtained at an S/C ratio of 3 to 1. Yield is defined as the ratio of the energy amount of output hydrogen and the energy consumption of input methane, and the related equation is shown in Equation (8). According to Kuhn's research, carbon deposition occurs when the S/C ratio is less than 2.5, and when the S/C ratio is more than 4, the heat load of heating water increases and efficiency decreases [46]. Therefore, the SC ratio was fixed at 3 for all subsequent simulations.

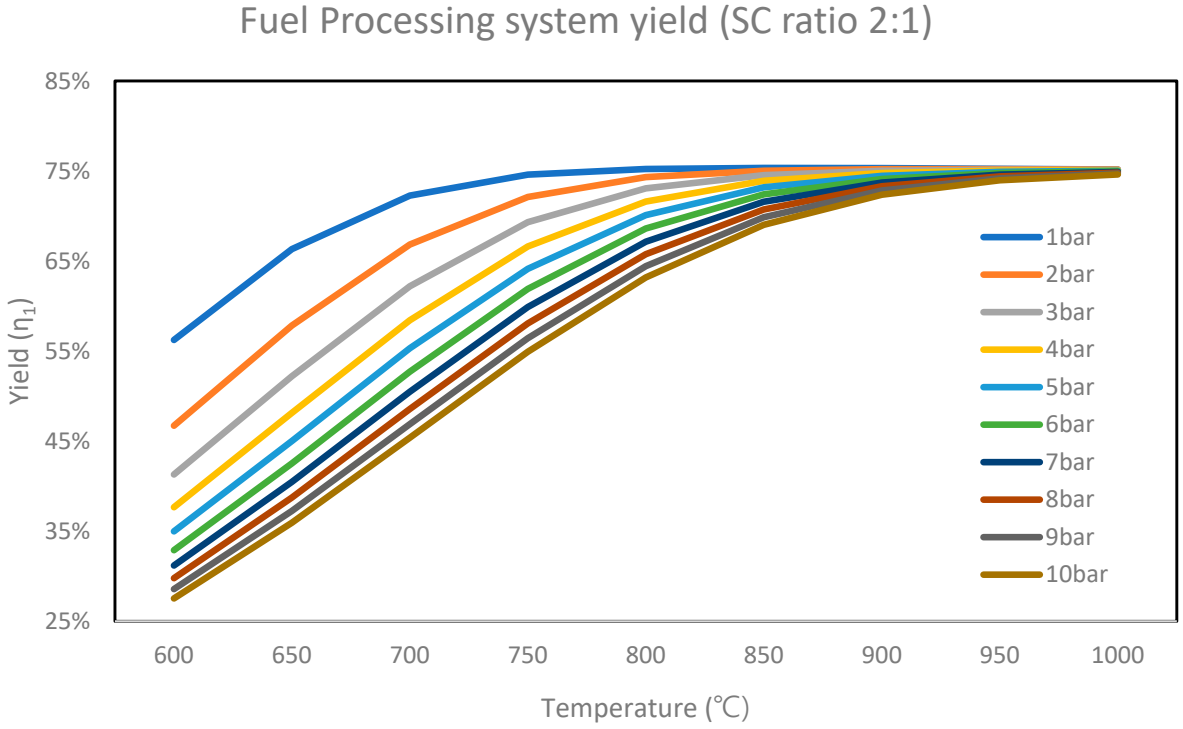

Figure 7. *Cont.*

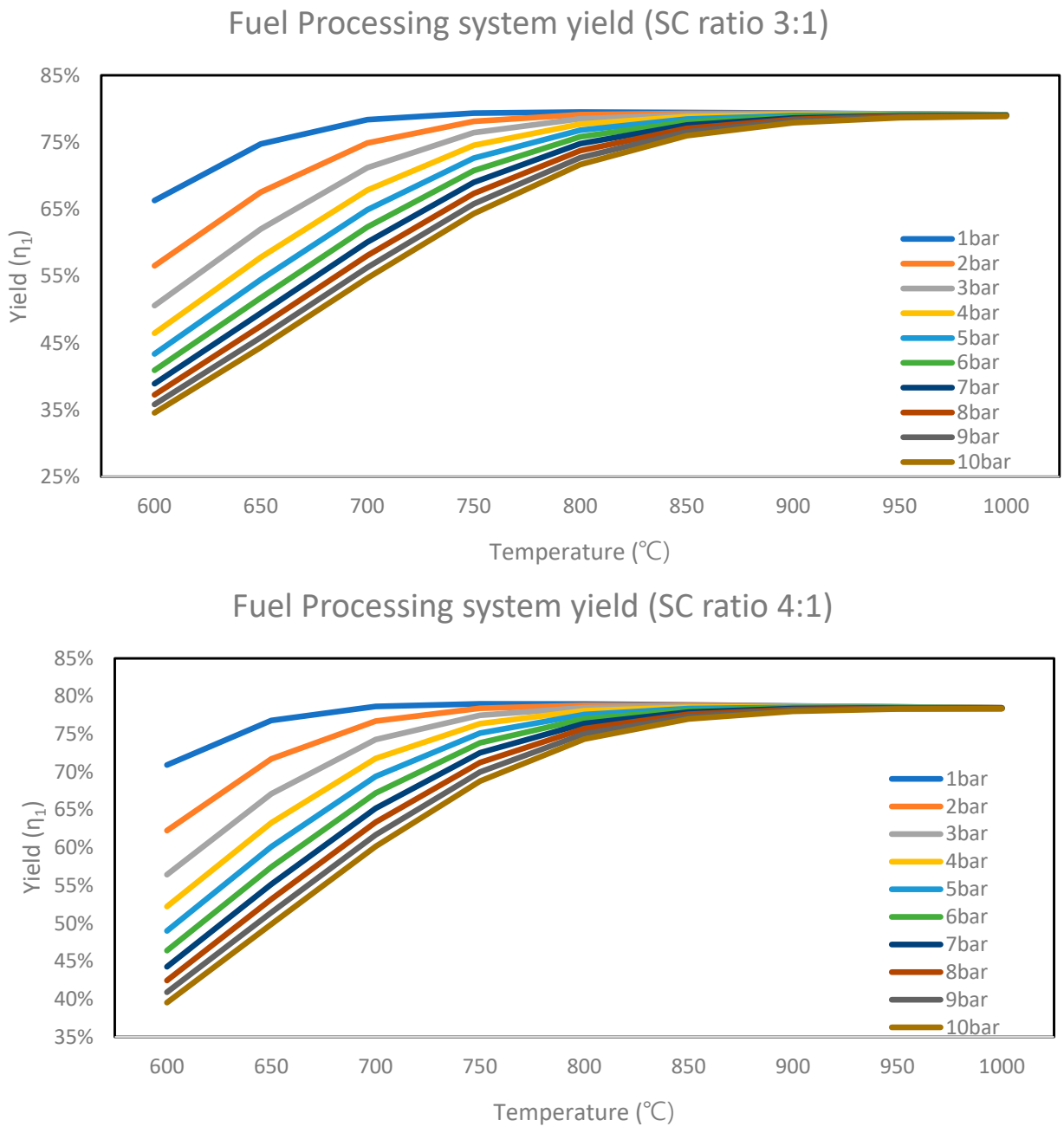

Figure 7. Fuel-processing system yield SC ratio.

9. Calculation of the Reformer Yield

The efficiency of the reformer-WGS system was analyzed using the Aspen Plus® simulation results. Figure 8 shows the calculated efficiency of the reformer-WGS system measured according to the reformer temperature change. The efficiency of the reformer system would be calculated as the ratio between the energy of produced hydrogen and the energy of supplied natural gas, which is shown in Equation (8) [16,17,42,43].

$$\eta_1 = \frac{LHV_{H_2} \times n_{H_2}(produced)}{LHV_{CH_4} \times (n_{CH_4}(burner) + n_{CH_4}(process))} \quad (8)$$

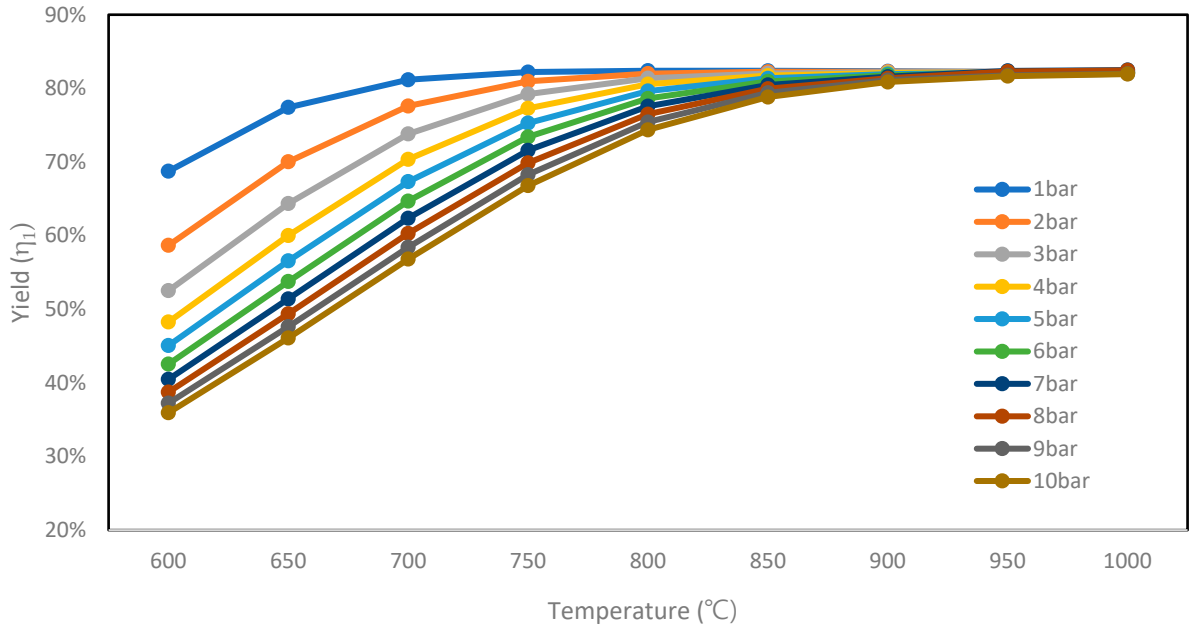

Figure 8. Fuel-processing system yield at various T and P for 10 kW H_2 production.

In Equation (8), $n_{H_2(produced)}$ is the flow rate of produced hydrogen (mol/s) in the fuel-processing system, $n_{CH_4(burner)}$ is the flow rate of the methane supplied to the burner, and $n_{CH_4(process)}$ is the flow rate of methane supplied to the reformer as a raw material. LHV H_2 and LHV CH_4 are the lower heating value of hydrogen mass at the outlet and the lower heating value of CH_4 at the inlet, respectively.

The fuel-processing system yields at various temperature and pressure conditions for 10 kW H_2 production were calculated using Equation (8) and are summarized in Figure 8. As the conversion of CH_4 increases, less PNG is needed to make 10 kW H_2, and the lower the conversion of CH_4, the more PNG is needed. The amount of BNG supplied to the system according to the conversion of CH_4 is shown in Figure 5. As shown in Figure 8, fuel-processing system yield increases and stabilizes with increasing temperature at a fixed pressure. In addition, under the same temperature conditions, as the pressure increased, the CH_4 conversion rate decreased according to Le Chatelier's law, resulting in a decrease in yield. The maximum yield is 82.40% at a pressure of 1 atm and a temperature of 800 °C, which is estimated at the highest CH_4 conversion under this condition.

10. PSA Simulation

The PSA system was simulated by the Aspen Adoption® simulator. In the simulation, the Peng–Robinson equation of state was employed for the calculation of the thermodynamic properties of gases, and the Langmuir isotherm was applied for the calculation of the adsorption equilibrium. The pressure change in the bed was calculated using the Ergun equation [47]. Product gas streams at a reformer temperature between 600 °C and 1000 °C in the fuel-processing system and at a system pressure between 1 atm and 9 atm were pressurized and supplied to the PSA system to purify H_2. During simulation, isothermal assumption was applied for the adsorption bed [48,49]. The overall process simulation of the PSA system is shown in Figure 9. Two adsorption beds were working in turns during the purification process, and impurities were removed from the inlet gas. For simulation, one-bed PSA simulation was conducted to determine the swing time under the two-bed condition. The switching time was determined at the time where the hydrogen concentration was 99.97% in the outlet stream of bed 1. An example of the simulation result of bed 1 is shown in Figure 10. In Figure 10, we can see that the swing time at which the concentration of hydrogen is 99.97% in the outlet stream is 16 s and is a function of the size of the adsorber and the properties of the adsorbent.

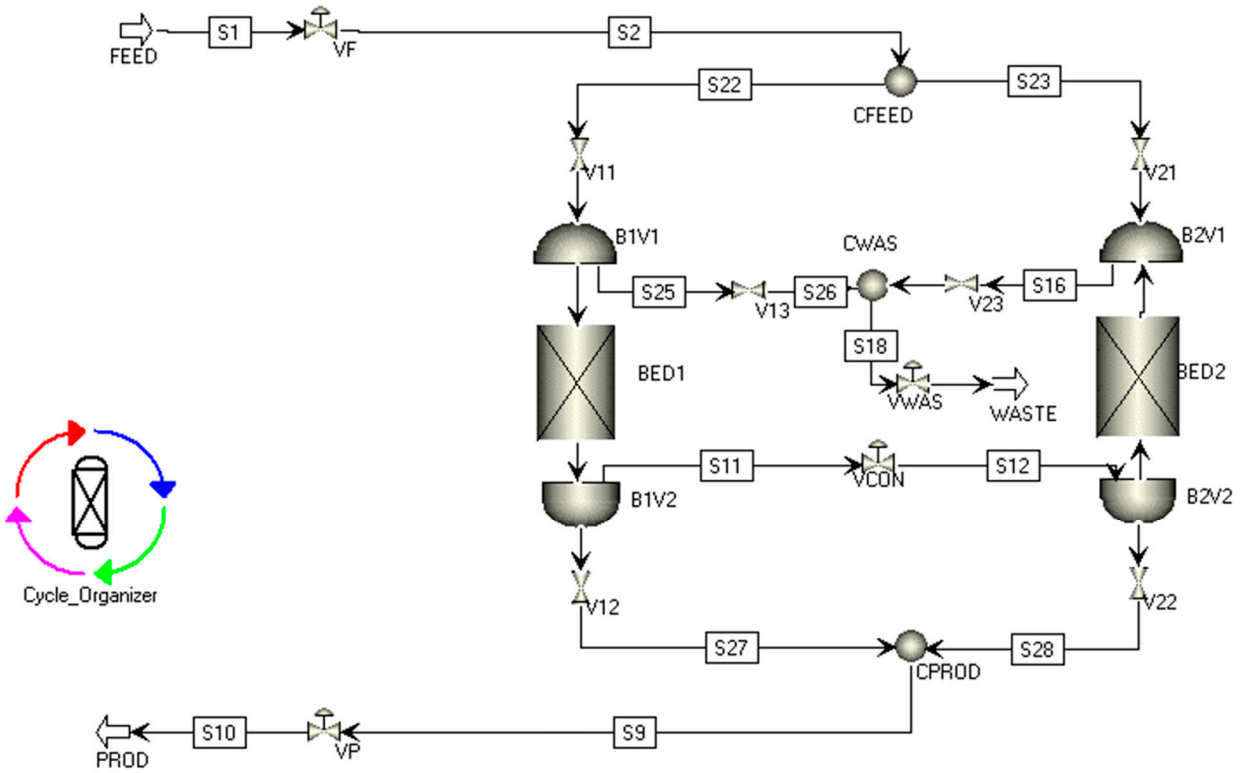

Figure 9. PSA flow sheet.

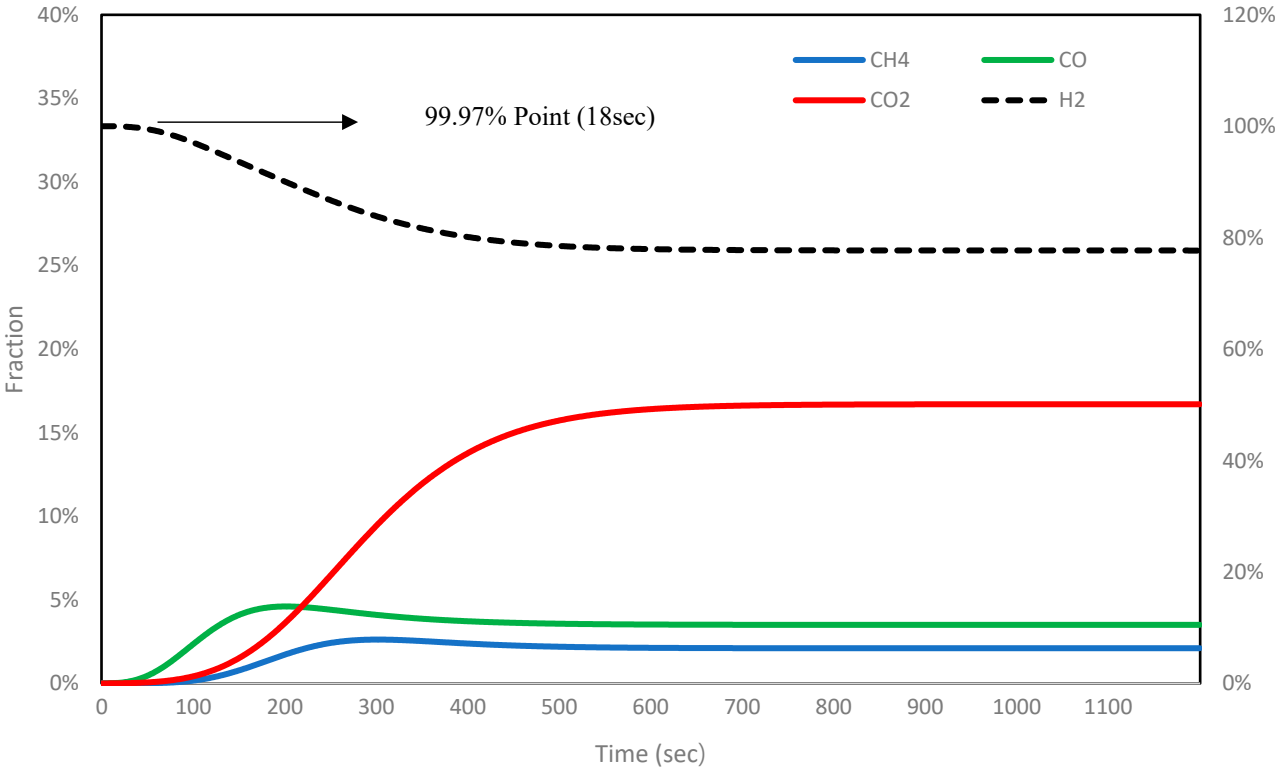

Figure 10. One-bed simulation example for determine switching time.

Two-bed PSA process simulation was also conducted, and the cycle of the PSA process is the following:

I. Bed 1 is filled with the inlet stream of PSA while bed 2 is blown down.
II. Impurities are adsorbed by bed 1 due to inlet gas continuously supplied to bed 1, while adsorbed impurities in bed 2 are desorbed and released from bed 2. After impurities are adsorbed, the hydrogen concentration at the outlet stream of bed 1 would be 99.97%.
III. After bed 1 is completely filled with impurities, the outlet stream of bed 1 is introduced to bed 2 to make the pressures of both beds equal.
IV. Bed 2 is filled with the inlet stream of PSA, while bed 1 is blown out.
V. Go to (i) and repeat the process after swinging bed 1 with 2.
VI. The cycle of the whole process is summarized in Table 5.

Table 5. PSA system cycle steps.

Step	Bed 1	Bed 2
1	Pressurize	Blow down
2	Adsorption	Purge
3	Depressurize	Pressure equalization
4	Blow down	Pressurize
5	Purge	Adsorption
6	Pressure equalization	Depressurize

For the simulation, a cylindrical bed was used, the length of the bed was 1 m, the diameter was 0.037 m, the adsorbent was assumed to be spherical, and the diameter was 0.0015 m. Langmuir parameters and bed parameters used in the simulation are shown in Table 3 [31].

The results of calculating the concentration change at the bed outlet after going through the above process are shown in Figure 11. As the adsorption process progresses during operation, the hydrogen concentration at the outlet of the adsorption bed decreases. The adsorption bed switches when the hydrogen concentration reaches 99.97%.

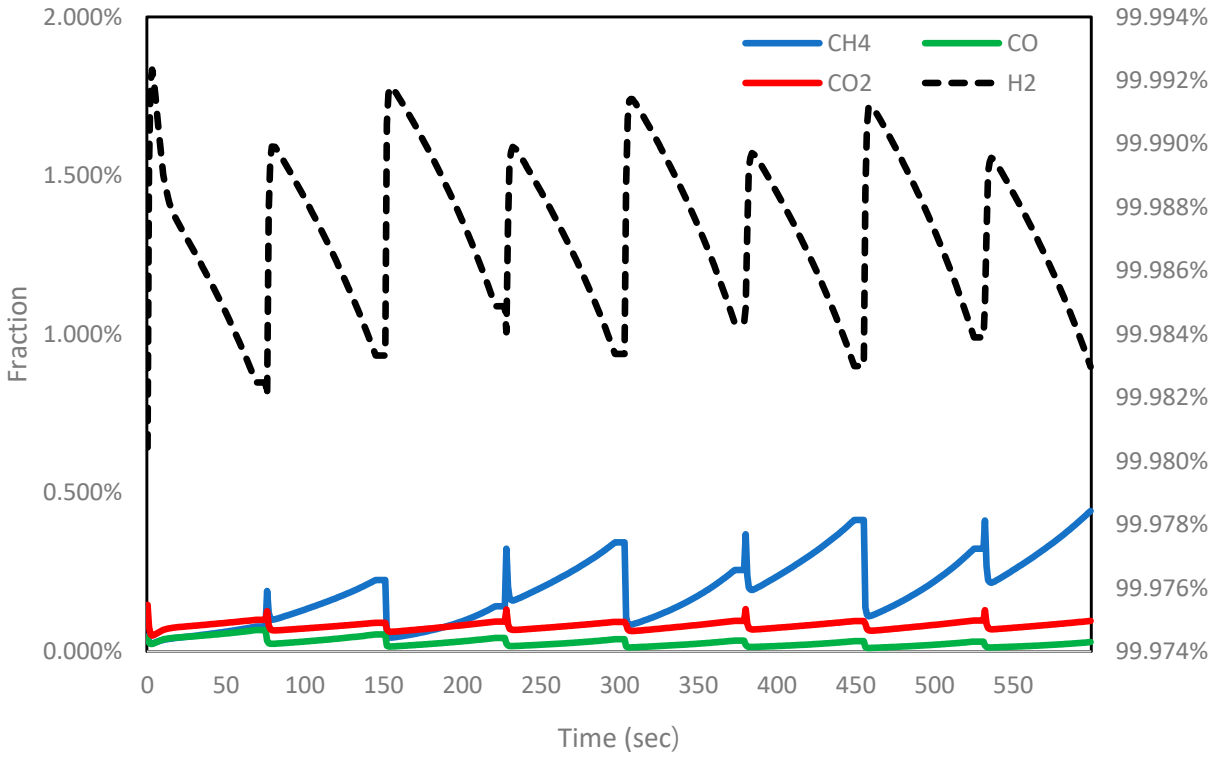

Figure 11. Two-bed system outlet composition.

The hydrogen-purification efficiency of the PSA system was defined as the ratio between the enthalpy of hydrogen at the PSA outlet stream to the enthalpy of hydrogen at the PSA inlet stream, as shown in Equation (9), and the result is summarized in Figure 12 [42,43].

$$\eta_2 = \frac{LHV_{H_2} \times n_{H_2}(PSA\ product\ gas)}{LHV_{H_2} \times n_{H_2}(PSA\ feed\ gas)} \quad (9)$$

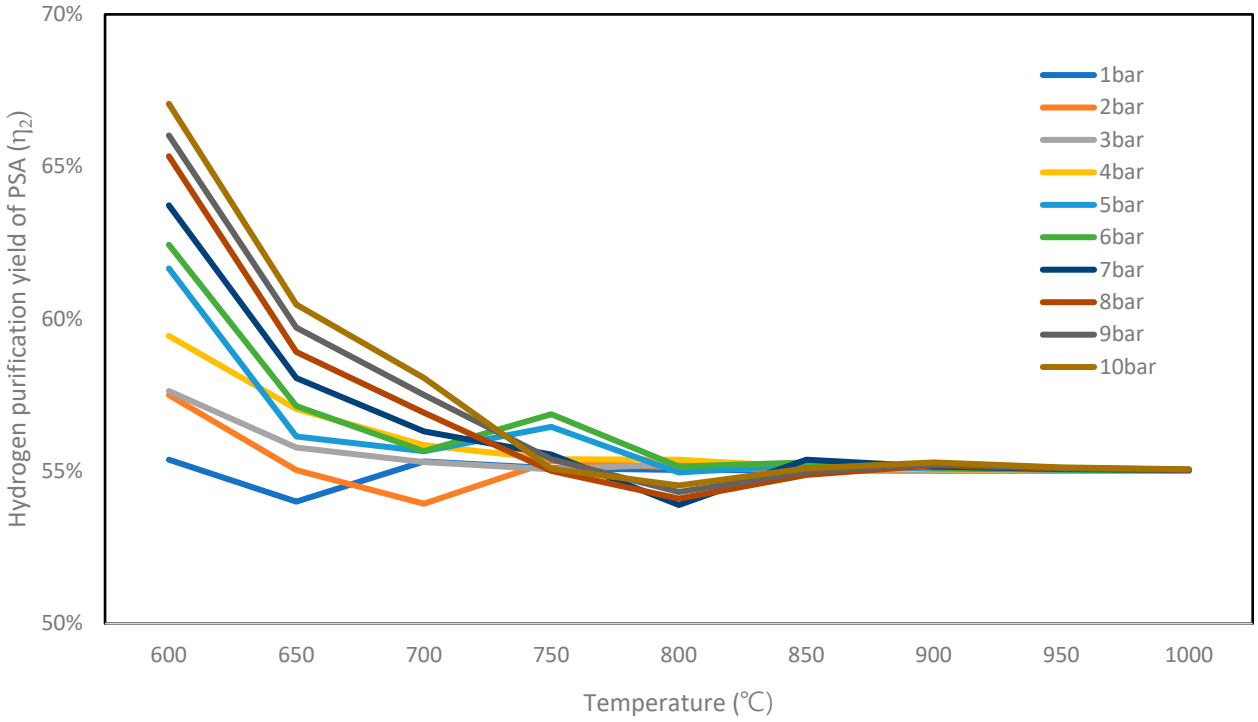

Figure 12. Hydrogen-purification yield of the PSA process.

As shown in Figure 12, the efficiency of the PSA system was constant at about 55% at reformer temperatures of about 850 °C and higher. The temperature at this time is the operating condition of the reformer, and the PSA yield was also measured as almost constant as the conversion ratio became almost constant after a specific temperature of about 850 °C (shown in Figure 4). At lower temperatures and higher-pressure conditions, the PSA yield is relatively higher since the amount of hydrogen produced in the fuel-processing system is smaller, and the amount of hydrogen purged with impurities from the PSA system is relatively small. This is the result of methane conversion, and when the methane conversion is low, the amount of input gas adsorbed is large, so the adsorption of hydrogen is relatively low and the measured yield is high. As a result, the yield would be higher, although the amount of hydrogen production is low.

11. Overall Yield

By definition, the efficiency of the overall system was calculated as the ratio of the enthalpy of hydrogen produced at the PSA outlet and the summation of the BNG enthalpy and the PNG enthalpy shown in Equation (10), with the results summarized in Figure 13.

$$\eta_3 = \frac{LHV_{H_2} \times n_{H_2}(produced)}{LHV_{CH_4} \times \left(n_{CH_4}(burner) + n_{CH_4}(process)\right) + Compressor\ work} \quad (10)$$

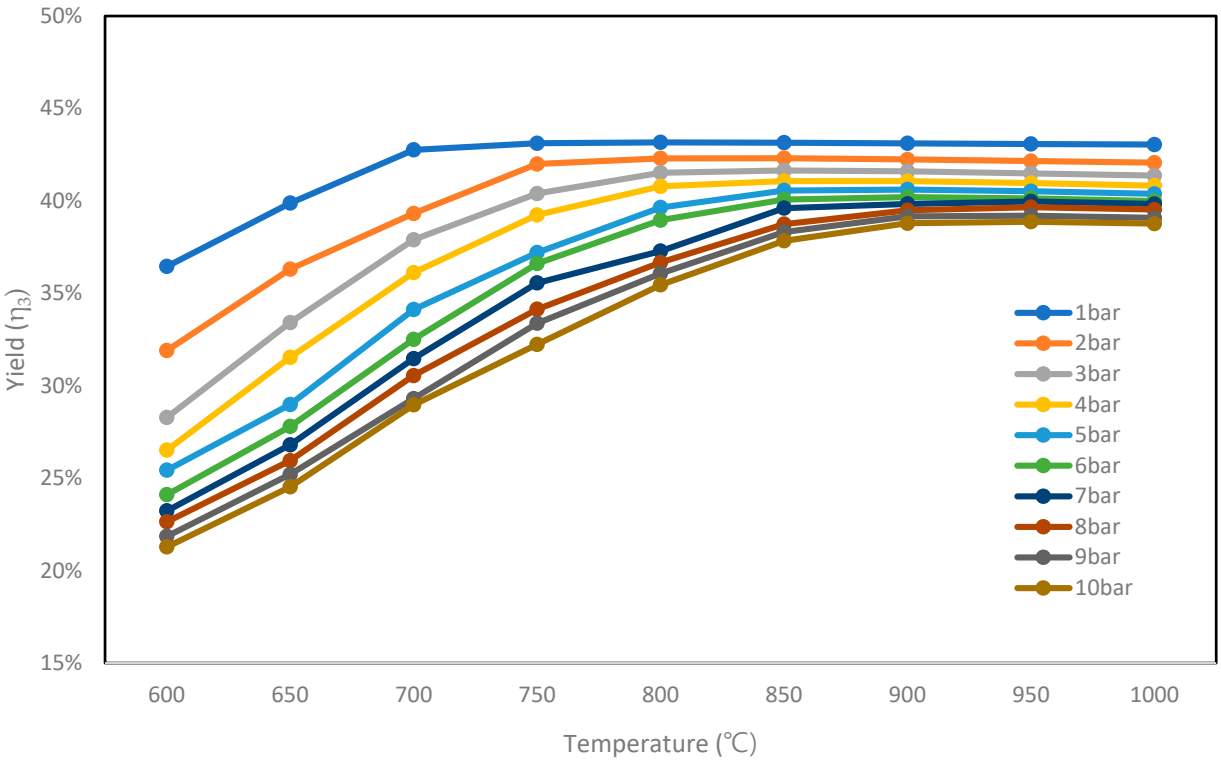

Figure 13. Overall system yield.

The overall system showed a maximum yield of about 43.17% at 1 atm and 800 °C. By adding compressor work to the yield of the existing fuel-processing system, the yield was reduced due to the process of pressurizing. Therefore, the highest efficiency was shown at 1 atm and 800 °C.

12. Analysis of Results

This study attempted to understand improvements of the pure-hydrogen-production system by observing the performance and sensitivity of the system according to load change in the reformer, the water–gas shift reactor, and the PSA, and analyzing the operation efficiency. Simulations were conducted at a temperature between 600 and 1000 °C at a reformer pressure of 1 atm and 10 atm for the fuel-processing system and conducted at a temperature of 15 °C and a pressure 9 atm for the PSA system. In the fuel-processing system, efficiency varies from 35.95% to 82.40% depending on temperature and pressure conditions, and the maximum efficiency was about 82.40% with reformer conditions of 800 °C and 1 atm. In the PSA system, efficiency varied between 55% and 67%, and the maximum efficiency was 67% at reformer conditions of 10 atm and 600 °C. The efficiency of the overall system ranged from 21.28% to 43.17% and the highest efficiency was 43.17% with reformer conditions of 800 °C and 1 atm. The most critical variable in these simulation results is assumed to be the input methane amount, denoted as PNG. Based on this, using the commercial software MATLAB R2023b®, 3D graphs depicting the overall yield according to temperature and pressure conditions of the reformer were generated at various temperature and pressure conditions (shown in Figure 14).

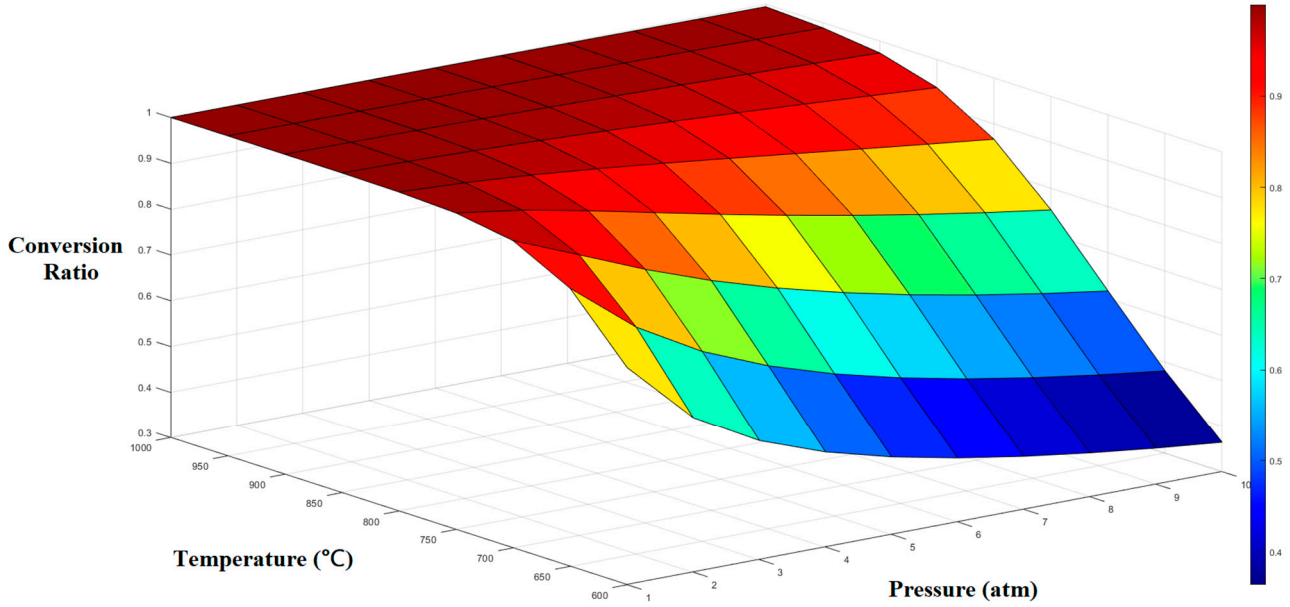

Figure 14. 3D graph of the methane-conversion ratio according to temperature and pressure.

As is shown in the figure, the methane conversion increases as temperature increases and pressure decreases. However, at a higher temperature, there is no noticeable difference in methane conversion as the reformer pressure changes. The empirical model for calculating the conversion of methane at given temperatures and pressures of the fuel-processing system is listed at Equation (11).

$$\begin{aligned} Conversion(T,P) = {} & -2.39 - 0.001365P + 0.008121 \times T + 1.39 \times 10^{-7}P^2 \\ & +1.269 \times 10^{-6}TP - 4.747 \times 10^{-6}T^2 \end{aligned} \quad (11)$$

where T is the temperature of the reformer reactor and P is the pressure of the fuel-processing system. The R^2 value of the empirical equation is 0.9805.

The overall yield of the whole system at various temperature and pressure conditions is summarized in Figure 15.

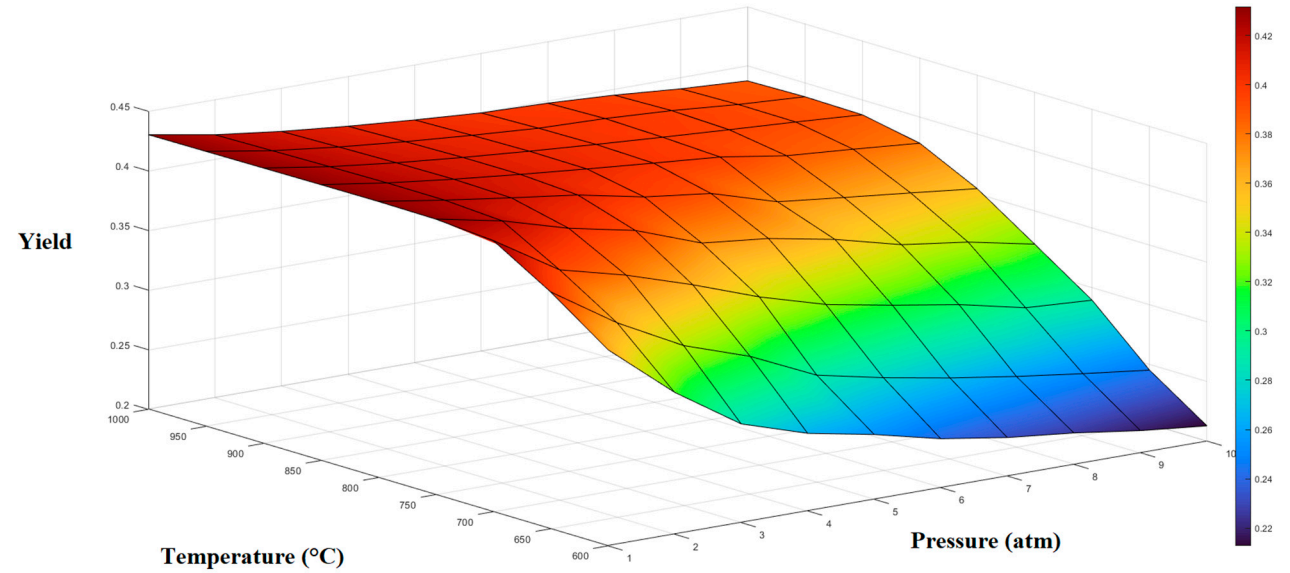

Figure 15. 3D overall yield of the combined fuel-processing system and the PSA system according to temperature and pressure.

The overall hydrogen-production yield is also higher at relatively high reformer temperatures and high reformer pressure conditions but stabilized at a higher temperature regardless of the reformer pressure. The hydrogen-production yield for the overall process was also obtained and is listed at Equation (12).

$$Yield(T,P) = -0.6163 - 0.0004557P + 0.002533T + 7.147 \times 10^{-8}P^2 + 3.514 \times 10^{-7}TP - 1.486 \times 10^{-6}T^2 \quad (12)$$

Using similar methods, new prediction equations for calculating methane conversion and yield calculations for other systems can be obtained from simulation results. These equations can be used to predict overall yield under various temperature and pressure conditions.

The fuel-processing system had the highest efficiency at 1 atm and 800 °C at the reformer, and the overall system considering the compressor and PSA had the highest efficiency at 1 atm and 800 °C. The overall yield was plotted as a function of conversion, which is shown in Figure 16.

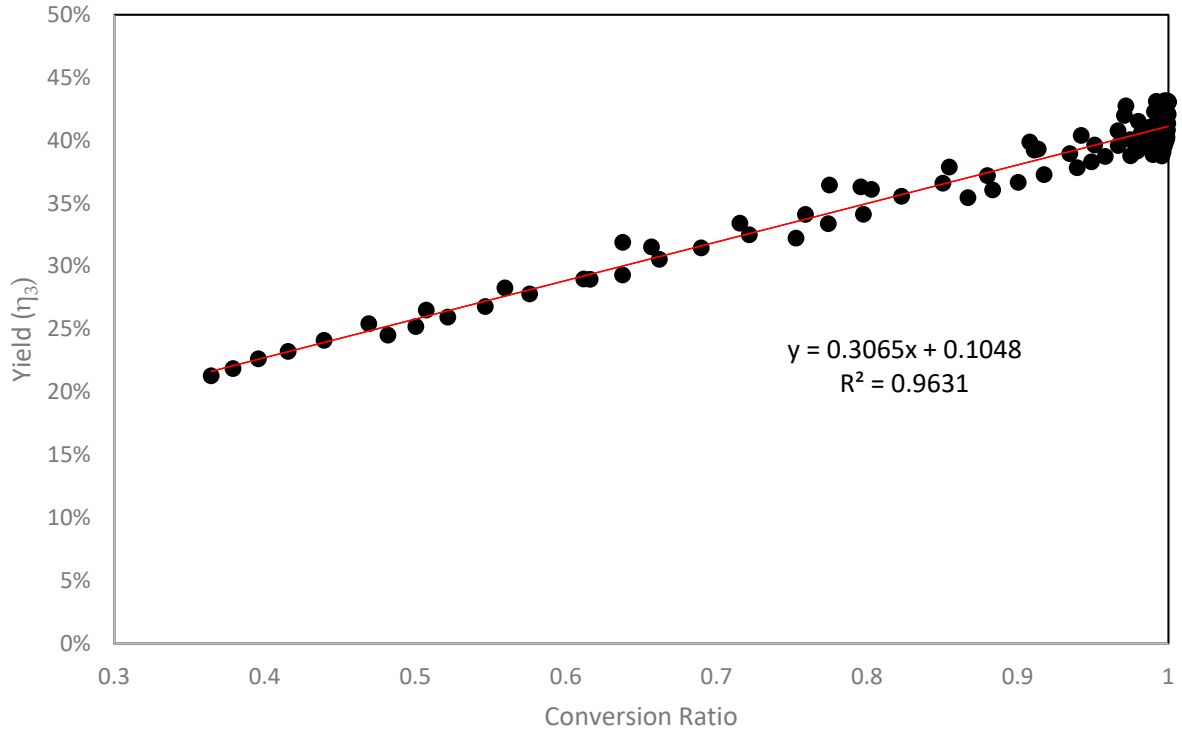

Figure 16. Overall yield according to the methane conversion.

As shown in Figure 16, overall yield linearly increases as methane conversion increases, and it is expressed as a linear function.

Equation (12) can be used to predict the overall yield of a combined processing system and the PSA system. In the combined system, the heat energy needed for the reaction is supplied by BNG and the compression work is conducted by two compressors. One is used to pressurize the inlet pressure of the reformer between 1 atm and 9 atm (compressor 1) and the other is used to pressurize the inlet pressure of the PSA to 9 atm (compressor 2). The compressors' work is organized according to the reformer pressure condition. The work of compressor 1 decreases as conversion increases since a lesser amount of PNG is needed at a higher conversion to make 10 kW hydrogen. It is also higher at high reformer pressure conditions. In Figure 17, the amount of PNG and the amount of BNG needed to make 10 kW hydrogen and the total compression work (work of compressor 1 and of compressor 2) are listed. As shown in the figure, the most energy needed for hydrogen production is PNG, and the least amount of energy supplied is compressor work.

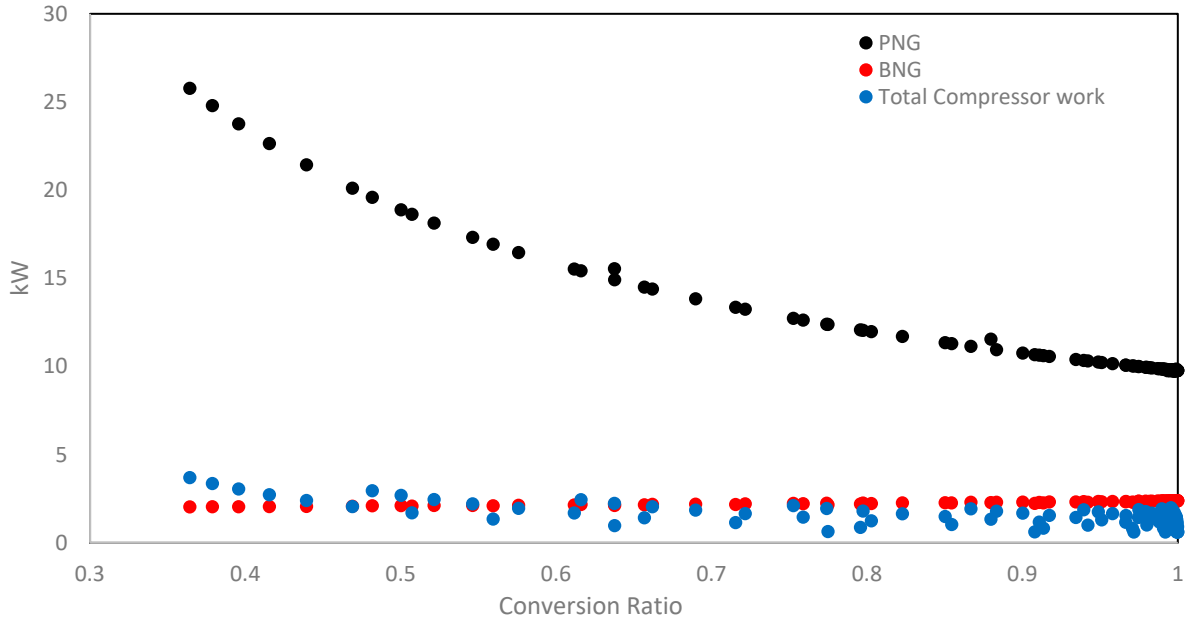

Figure 17. Amount of each energy supplied to make 10 kW hydrogen according to the methane conversion.

The amount of each energy supplied at different overall yields is also shown in Figure 18.

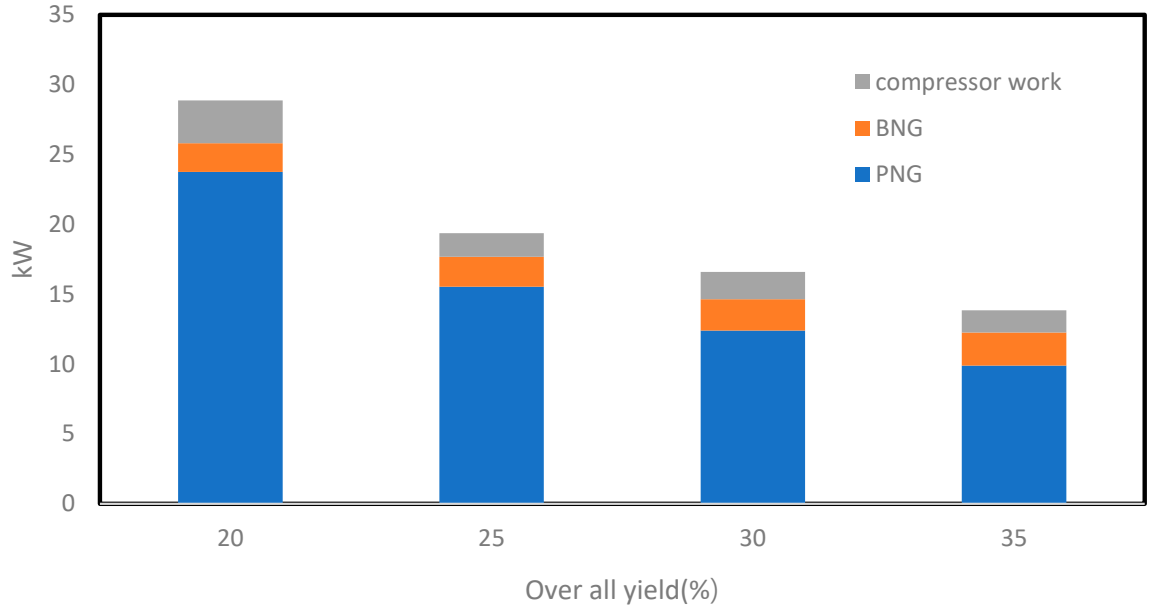

Figure 18. Amount of energy supplied according to the overall yield.

In Figure 18, the amount of PNG supplied, and the compression work decrease rapidly as overall yield increases, while the small amount of BNG supplied decreases as overall yield increases.

13. Conclusions

A combined system of a fuel-processing system connected with a PSA system to produce 1 kW pure hydrogen was simulated using Aspen Plus® and Aspen Adsorption® simulators. The reformer was operated at a temperature of 600 °C to 100 °C and at a pressure of 1 atm to 9 atm. The water–gas shift reactor was operated at 200 °C and the

same as the reformer pressure, and the PSA system was operated at 15 °C and 9 atm. For energy analysis, all energies are expressed as a function of methane conversion. From the simulation data, a prediction equation was created to calculate the methane-conversion rate and the overall hydrogen-production yield under various temperature and pressure conditions. For a real system, methane conversion can be calculated from experimental data; overall yield can also be calculated using similar methods, and the operating conditions are determined to achieve the maximum hydrogen-production yield. The amount of natural gas and the energy needed for each unit is expressed as a function of methane conversion. As a result, overall system yield was a linear function of methane conversion. The maximum yield for the fuel-processing system was 82.40% at a reformer temperature of 800 °C and a system pressure of 1 atm, and the maximum yield for the PSA system was 55% at an 850 °C reformer temperature. The overall yield was 43.17% at 800 °C and 1 atm in the reformer.

Author Contributions: Methodology, S.L.; Formal analysis, S.K.; Investigation, S.K.; Writing—original draft, S.K.; Writing—review & editing, S.L.; Supervision, S.L.; Project administration, S.L.; Funding acquisition, S.L. All authors have read and agreed to the published version of the manuscript.

Funding: The authors are thankful to the Korea Institute of Energy Technology Evaluation and Planning (KETEP) for the support grant funded by the Korea government Ministry of Trade, Industry and Energy under the project titled: "Development on localization technologies of export-purposed stationary fuel cell systems", numbered: 20183010032400, "Fuel cell safety demonstration linked to hydrogen extractor for public buildings", numbered: 20203040030110.

Conflicts of Interest: The authors declare no conflict of interest. The funders had no role in the design of the study; in the collection, analyses, or interpretation of data; in the writing of the manuscript; or in the decision to publish the results.

References

1. Adamson, K.-A. *Stationary Fuel Cells: An Overview*; Elsevier: Amsterdam, The Netherlands, 2010.
2. Pérez-Lombard, L.; Ortiz, J.; Pout, C. A review on buildings energy consumption information. *Energy Build.* **2008**, *40*, 394–398. [CrossRef]
3. Environmental Sciences Division ORNL. *Global, Regional, and National Fossil-Fuel CO_2 Emissions*; Environmental Sciences Division ORNL: Oak Ridge, TN, USA, 2010. [CrossRef]
4. Labis, P.E.; Visande, R.G.; Pallugna, R.C.; Caliao, N.D. The contribution of renewable distributed generation in mitigating carbon dioxide emissions. *Renew. Sustain. Energy Rev.* **2011**, *15*, 4891–4896. [CrossRef]
5. Bilgen, S. Structure and environmental impact of global energy consumption. *Renew. Sustain. Energy Rev.* **2014**, *38*, 890–902. [CrossRef]
6. Abdmouleh, Z.; Gastli, A.; Ben-Brahim, L.; Haouari, M.; Al-Emadi, N.A. Review of optimization techniques applied for the integration of distributed generation from renewable energy sources. *Renew. Energy* **2017**, *113*, 266–280. [CrossRef]
7. Ackermann, T. Distributed generation: A definition. *Electr. Power Syst. Res.* **2001**, *57*, 195–204. [CrossRef]
8. Sun, L.; Jin, Y.; Pan, L.; Shen, J.; Lee, K.Y. Efficiency analysis and control of a grid-connected PEM fuel cell in distributed generation. *Energy Convers. Manag.* **2019**, *195*, 587–596. [CrossRef]
9. Dorer, V.; Weber, R.; Weber, A. Performance assessment of fuel cell micro-cogeneration systems for residential buildings. *Energy Build.* **2005**, *37*, 1132–1146. [CrossRef]
10. Willis, H.L. *Distributed Power Generation: Planning and Evaluation*; CRC Press: Boca Raton, FL, USA, 2018.
11. Pepermans, G.; Driesen, J.; Haeseldonckx, D.; Belmans, R.; D'haeseleer, W. Distributed generation: Definition, benefits and issues. *Energy Policy* **2005**, *33*, 787–798. [CrossRef]
12. Soltani, R.; Rosen, M.A.; Dincer, I. Assessment of CO_2 capture options from various points in steam methane reforming for hydrogen production. *Int. J. Hydrogen Energy* **2014**, *39*, 20266–20275. [CrossRef]
13. Sorensen, B.; Spazzafumo, G. *Hydrogen and Fuel Cells: Emerging Technologies and Applications*; Academic Press: Cambridge, MA, USA, 2018.
14. Haseli, Y. Maximum conversion efficiency of hydrogen fuel cells. *Int. J. Hydrogen Energy* **2018**, *43*, 9015–9021. [CrossRef]
15. Rosli, R.E.; Sulong, A.B.; Daud, W.R.W.; Zulkifley, M.A.; Husaini, T.; Rosli, M.I.; Majlan, E.H.; Haque, M.A. A review of high-temperature proton exchange membrane fuel cell (HT-PEMFC) system. *Int. J. Hydrogen Energy* **2017**, *42*, 9293–9314. [CrossRef]
16. Braga, L.B.; Silveira, J.L.; da Silva, M.E.; Tuna, C.E.; Machin, E.B.; Pedroso, D.T. Hydrogen production by biogas steam reforming: A technical, economic and ecological analysis. *Renew. Sustain. Energy Rev.* **2013**, *28*, 166–173. [CrossRef]
17. Sharaf, O.Z.; Orhan, M.F. An overview of fuel cell technology: Fundamentals and applications. *Renew. Sustain. Energy Rev.* **2014**, *32*, 810–853. [CrossRef]

18. Larminie, J.; Dicks, A.; McDonald, M.S. *Fuel Cell Systems Explained*, 2nd ed.; John Wiley & Sons Ltd.: Hoboken, NJ, USA, 2003; ISBN 047084857X.
19. Pen, A.; Gómez, M.; Fierro, J. New catalytic routes for syngas and hydrogen production. *Appl. Catal. A Gen.* **1996**, *144*, 7–57. [CrossRef]
20. Kolb, G. *Fuel Processing: For Fuel Cells*; John Wiley & Sons: Hoboken, NJ, USA, 2008.
21. Yang, S.-I.; Choi, D.-Y.; Jang, S.-C.; Kim, S.-H.; Choi, D.-K. Hydrogen separation by multi-bed pressure swing adsorption of synthesis gas. *Adsorption* **2008**, *14*, 583–590. [CrossRef]
22. Izquierdo, U.; Barrio, V.; Cambra, J.; Requies, J.; Güemez, M.; Arias, P.; Kolb, G.; Zapf, R.; Gutiérrez, A.; Arraibi, J. Hydrogen production from methane and natural gas steam reforming in conventional and microreactor reaction systems. *Int. J. Hydrogen Energy* **2012**, *37*, 7026–7033. [CrossRef]
23. LeValley, T.L.; Richard, A.R.; Fan, M. The progress in water gas shift and steam reforming hydrogen production technologies—A review. *Int. J. Hydrogen Energy* **2014**, *39*, 16983–17000. [CrossRef]
24. Seo, Y.T.; Seo, D.J.; Jeong, J.H.; Yoon, W.L. Design of an integrated fuel processor for residential PEMFCs applications. *J. Power Sources* **2006**, *160*, 505–509. [CrossRef]
25. Qi, Z.; He, C.; Kaufman, A. Effect of CO in the anode fuel on the performance of PEM fuel cell cathode. *J. Power Sources* **2002**, *111*, 239–247. [CrossRef]
26. Rasheed, R.K.A.; Chan, S.H. Transient carbon monoxide poisoning kinetics during warm-up period of a high-temperature PEMFC—Physical model and parametric study. *Appl. Energy* **2014**, *140*, 44–51. [CrossRef]
27. Yang, R. Gas Separation by Adsorption Processes. *Chem. Eng. Sci.* **1988**, *43*, 985. [CrossRef]
28. Jiménez, S.; Soler, J.; Valenzuela, R.; Daza, L. Assessment of the performance of a PEMFC in the presence of CO. *J. Power Sources* **2005**, *151*, 69–73. [CrossRef]
29. Díaz, M.A.; Iranzo, A.; Rosa, F.; Isorna, F.; López, E.; Bolivar, J.P. Effect of carbon dioxide on the contamination of low temperature and high temperature PEM (polymer electrolyte membrane) fuel cells. Influence of temperature, relative humidity and analysis of regeneration processes. *Energy* **2015**, *90*, 299–309. [CrossRef]
30. Amphlett, J.C.; Mann, R.F.; Pepplely, B.A. On board hydrogen purification for steam reformatton/pem fuel cell vehicle power plants. *Int. J. Hydrogen Energy* **1996**, *21*, 673–678. [CrossRef]
31. You, Y.-W.; Lee, D.-G.; Yoon, K.-Y.; Moon, D.-K.; Kim, S.M.; Lee, C.-H. H2 PSA purifier for CO removal from hydrogen mixtures. *Int. J. Hydrogen Energy* **2012**, *37*, 18175–18186. [CrossRef]
32. Riboldi, L.; Bolland, O. Overview on Pressure Swing Adsorption (PSA) as CO_2 Capture Technology: State-of-the-Art, Limits and Potentials. *Energy Procedia* **2017**, *114*, 2390–2400. [CrossRef]
33. Du, Z.; Liu, C.; Zhai, J.; Guo, X.; Xiong, Y.; Su, W.; He, G. A Review of Hydrogen Purification Technologies for Fuel Cell Vehicles. *Catalysts* **2021**, *11*, 393. [CrossRef]
34. Pasdag, O.; Kvasnicka, A.; Steffen, M.; Heinzel, A. Highly Integrated Steam Reforming Fuel Processor with Condensing Burner Technology for Maximised Electrical Efficiency of CHP-PEMFC Systems. *Energy Procedia* **2012**, *28*, 57–65. [CrossRef]
35. Chen, S.; Pei, C.; Gong, J. Insights into interface engineering in steam reforming reactions for hydrogen production. *Energy Environ. Sci.* **2019**, *12*, 3473–3495. [CrossRef]
36. Patel, K.S.; Sunol, A.K. Modeling and simulation of methane steam reforming in a thermally coupled membrane reactor. *Int. J. Hydrogen Energy* **2007**, *32*, 2344–2358. [CrossRef]
37. Amran, U.I.; Ahmad, A.; Othman, M.R. Kinetic based simulation of methane steam reforming and water gas shift for hydro-gen production using aspen plus. *Chem. Eng. Trans.* **2017**, *56*, 1681–1686. [CrossRef]
38. Xu, J.; Froment, G.F. Methane steam reforming, methanation and water-gas shift: I. Intrinsic kinetics. *AIChE J.* **1989**, *35*, 88–96. [CrossRef]
39. Twigg, M.V. *Catalyst Handbook*, 2nd ed.; Taylor & Francis: Abingdon, UK, 1989.
40. Newsome, D.S. The Water-Gas Shift Reaction. *Catal. Rev.* **1980**, *21*, 275–318. [CrossRef]
41. Meloni, E.; Martino, M.; Palma, V. A Short Review on Ni Based Catalysts and Related Engineering Issues for Methane Steam Reforming. In Proceedings of the 5th Global Conference on Catalysis, Chemical Engineering, and Technology (CAT), London, UK, 16–18 September 2019; p. 352.
42. Ho, M.T.; Allinson, G.W.; Wiley, D.E. Reducing the Cost of CO_2 Capture from Flue Gases Using Pressure Swing Adsorption. *Ind. Eng. Chem. Res.* **2008**, *47*, 4883–4890. [CrossRef]
43. Raganati, F.; Alfe, M.; Gargiulo, V.; Chirone, R.; Ammendola, P. Isotherms and thermodynamics of CO_2 adsorption on a novel carbon-magnetite composite sorbent. *Chem. Eng. Res. Des.* **2018**, *134*, 540–552. [CrossRef]
44. Xiao, J.; Peng, Y.; Bénard, P.; Chahine, R. Thermal effects on breakthrough curves of pressure swing adsorption for hydrogen purification. *Int. J. Hydrogen Energy* **2016**, *41*, 8236–8245. [CrossRef]
45. Liu, Z.; Karimi, I. Simulation of a combined cycle gas turbine power plant in Aspen HYSYS. *Energy Procedia* **2019**, *158*, 3620–3625. [CrossRef]
46. Kuhn, J.; Kesler, O. Carbon deposition thresholds on nickel-based solid oxide fuel cell anodes II. Steam: Carbon ratio and current density. *J. Power Sources* **2015**, *277*, 455–463. [CrossRef]
47. Asgari, M.; Anisi, H.; Mohammadi, H.; Sadighi, S. Designing a commercial scale pressure swing adsorber for hydrogen purifica-tion. *Pet. Coal* **2014**, *56*, 552–561.

48. Lee, J.; Kim, M.; Lee, D.; Ahn, H.; Kim, M.; Lee, C. Heat-exchange pressure swing adsorption process for hydrogen separation. *AIChE J.* **2008**, *54*, 2054–2064. [CrossRef]
49. Abdeljaoued, A.; Relvas, F.; Mendes, A.; Chahbani, M.H. Simulation and experimental results of a PSA process for production of hydrogen used in fuel cells. *J. Environ. Chem. Eng.* **2018**, *6*, 338–355. [CrossRef]

Disclaimer/Publisher's Note: The statements, opinions and data contained in all publications are solely those of the individual author(s) and contributor(s) and not of MDPI and/or the editor(s). MDPI and/or the editor(s) disclaim responsibility for any injury to people or property resulting from any ideas, methods, instructions or products referred to in the content.